DYNAMIC FRACTURE PROPAGATION RESISTANCE EVALUATION ON DROP WEIGHT TEAR TEST LIKE SPECIMENS AT INSTRUMENTED HIGH VELOCITY IMPACT TESTS, APPLYING A GASGUN.

H.C. VAN ELST *

Using as striker a cylindrical high strength steel projectile (of 600 mm length and 40 mm diameter, mass 5.8 kg), ejected by a gasgun (at velocities up to 80 ms^{-1}, SENB ("drop weight tear test like")-specimens (of 100 mm length, 50 mm thickness and supported on a span of 400 mm) were separated by impact. The striker displacement, the rotational velocity of the SENB-specimen, the momentum transfer to the supports and the crack length could be recorded in time by suitable instrumentation, using a photocell array, a laser-Doppler technique, straingauges and high speed photography resp. From energy balance considerations the dissipated energy at separation and as a function of crack extension could be calculated. J_{1c} and $J/\Delta a$-curves could be determined for the relevant limit moment situation.

INTRODUCTION

In a previous paper{Van Elst (1)}the evaluation of the fracture propagation resistance from impact testing of SENB (drop weight tear test like) specimens, using a projectile ejected by a gasgun as striker and applying suitable instrumentation, was described. The same experimental technique was applied in this investigation, while moreover a laser-Doppler technique was used in addition to record two (displacement) velocities in x- and y-direction or both in x-direction at the specimen surface in two (sometimes one) fixed laboratory system positions (position) resp., situated at the surface of a specimen half in its original rest state. This appeared more promising for assessment of the kinetic energy of the impacted specimen required for the envisaged energy balance analysis than the (previously applied time consuming) method, in which the angular velocity had to be deduced from the high speed photography recorded angles of rotation in time of the specimen in order to find its (rotational) kinetic energy. High speed photography was applied as before to record the crack extension. The determination of the kinetic energy in time of the impacted specimen from the laser-Doppler technique recordings is elaborated below and in Van Elst (2).

MATERIAL AND SPECIMENS

50 mm thickness steelplates of a low alloy structural steel Fe510 (code 659K), conforming to B.S. 1501-281 A and a 5% Ni structural steel HY130 were investigated as to their dynamic fracture propagation resistance.
Drop weight tear test like SENB-specimens from both available steelplates were prepared with 100 mm width, 50 mm thickness (cf. Fig. 1) and 450 mm length for the Fe510 steel and 440 mm length for the HY130 steel resp.; the span was 400 mm. The Fe510 steel plate specimens were provided with a

*Metal Research Institute TNO, P.O.B. 541, 7300 AM APELDOORN, The Netherlands.

fatigued notch tip. The HY130 steel plate specimens had a machined notch with width 0.3 mm (at the tip). The geometry and dimensions of the striker used for impact testing (a cylindrical projectile ejected by a gasgun at velocities up to 80 mm^{-1}) and those of the specimens are shown in Fig. 1.

DYNAMICS OF SOLID BODY MODEL OF IMPACTED SENB-SPECIMEN IN VIEW OF APPLIED RECORDINGS TECHNIQUES

The topography of the impacted specimen is illustrated in Fig. 2; its kinematics are elaborated in Appendix I.
For the momentum in striker direction obtained by the specimen is assumed:

$$1^o.\ 2m\dot y_{Z_1} = \int_o^t P_p\,dt = M(V_o-V)t/\tau_p \text{ for } o \leq t \leq \tau_p; \quad (1.1)$$

τ_p = duration of impact on supported SENB-specimen hit at t=o by striker with velocity V_o and with velocity V after impact.

(It is thus assumed that the momentum transfer $M(V_o-V)$ proceeds linearly in time and the force P_p on the specimen remains constant during the impact of projectile and specimen.)

$$2^o.\ 2m\dot y_{Z_1} = M(V_o-V) \text{ for } \tau_p \leq t \leq t_i; \quad (1.2)$$

t_i = start of impact on supports by specimen.

$$3^o.\ 2m\dot y_{Z_1} = M(V_o-V)-\int_{t_i}^{t-t_i} P_s\,dt \text{ for } t_i \leq t \leq t_i+\tau_s; \quad (1.3)$$

τ_s=duration of impact on supports, hit at $t=t_i$ by specimen with momentum $M(V_o-V)$ in striker direction; $P_s=P_{s,L}+P_{s,R}$=sum of the forces on the two supports to be read from suitable straingauges responses on the supports.

$$4^o.\ 2m\dot y_{Z_1} = M(V_o-V)-2p_s \text{ for } t_i+\tau_s \leq t^*; \quad (1.4)$$

with $2p_s = P_{s,L} + P_{s,R} = \int_{t_i}^{t_i+\tau_s} P_s dt$ (and t^* = time of next impact)

y_{Z_1} follows from the equations 1 for $\dot y_{Z_1}$ as: $y_{Z_1}(t) = \int_o^t \dot y_{Z_1} dt$ (2)

If $\dot x_1$ and $\dot x_2$ are measured in (x_1,y_1) and (x_2,y_2) resp. then $\dot x_{Z_1}$ is offered (by AI-6) as:

$$\dot x_{Z_1} = \{\dot x_1(y_{Z_1} - y_2)-\dot x_2(y_{Z_1}-y)\}/(y_1-y_2) \quad (3.1)$$

The kinetic energy $E_{kin}/2$ obtained by specimen half 1 will be:

$$E_{kin}/2 = \tfrac{1}{2}m\dot y_{Z_1}^2 + \tfrac{1}{2}m\dot x_{Z_1}^2 + \tfrac{1}{2}T_1\dot\phi^2 \quad (4)$$

with T_1 = moment of inertia of specimen half 1 w.r.t. axis in thickness direction through its centre of gravity in Z_1: $T_1=bs(\ell^3w+w^3\ell)/12=m(\ell^2+w^2)/12$; (s = mass density of specimen material = $m/\ell wb$)

In 4, $\dot y_{Z_1}$ is given by 1 ; $\dot x_{Z_1}$ is given by 3.1; $\dot\phi$ is given by (cf. Fig.3 and AI-3 in Appendix I):

$$\dot\phi = (\dot x_1-\dot x_2)/(y_1-y_2)\ ;\ \dot\phi = (\dot y_3-\dot y_4)/(x_4-x_3) \quad (5)$$

The total energy balance reads: $\tfrac{1}{2}MV_o^2 = \tfrac{1}{2}MV^2+E_{kin}+E_{elast}+E_{diss}$ (6.1)

$$\tfrac{1}{2}MV_o^2 = \tfrac{1}{2}MV^2+E_{transl}+E_{vib}+E_{rot}+E_{elast}+E_{diss} \quad (6.2)$$

with: $E_{transl} = m\dot y_{Z_1}^2$; $E_{vib} = m\dot x_{Z_1}^2$; $E_{rot} = T_1\dot\phi^2$

Note that E_{vib} and E_{rot} have zero algebraic momentum and angular momentum resp.; the specimen halves exert equal forces and moment on each other.

$E_{diss} = \int_{a=a_o}^{w} R(a)da$; $E_{elast} \simeq (\ell-q)^2\phi^2/2C(a)$ (i.e. for E_{elast} a static estimate is given, with C(a) = elastic compliance for physical cracklength a, as in fact relevant in the quasi static case at unloading). E_{elast} is negligible compared to the other terms in 6.2; Van Elst and Lont (2).
In (x_1,y_1) and (x_2,y_2) at the surface of specimen half 1, velocities were measured using a laser-Doppler technique (on which is elaborated in Appendix II). If $\dot x_1$ and $\dot x_2$ are measured in (x_1,y_1) and (x_2,y_2) resp. then the equations 1,2,3,5, directly allow to find E_{kin}, as y_{Z_1} follows from 2, while from 3.1:

$$x_{Z_1} = \int_o^t \dot x_{Z_1} dt \quad (7.1)$$

If $\dot y_1$ and $\dot x_2$ are measured in (x_1,y_1) and (x_2,y_2) resp. then (from AI-2 in Appendix I) considering (x_2,y_2) and (x_{Z_1},y_{Z_1}) : $\dot\phi = (\dot x_2-\dot x_{Z_1})/(y_2-y_{Z_1})$ and considering (x_1,y_1) and (x_{Z_1},y_{Z_1}) : $\dot\phi = (\dot y_1-\dot y_{Z_1})/(x_{Z_1}-x_1)$.

$$\text{Thus: } \dot x_{Z_1} = \dot x_2-(y_2-y_{Z_1})(\dot y_1-\dot y_{Z_1})/(x_{Z_1}-x_1) \quad (3.2.1)$$

$$x_{Z_1}(t) = x_{Z_1}(t-\Delta t)+\bar{\dot x}_{Z_1}(t^*)\Delta t,$$

while $x_{Z_1}(o) = \frac{\ell}{2}$; $\bar{\dot x}_{Z_1}(t^*) \simeq \{\dot x_{Z_1}(t-\Delta t)+\dot x_{Z_1}(t)\}/2$ (7.2)

with $t^*\simeq t-\tfrac{1}{2}\Delta t$; $x_{Z_1}(t)$ can thus be found by "stepwise integration" from 3.2.1.

$\dot x_{Z_1}(t)^2+\dot x_{Z_1}(t)\zeta+\eta+\psi\frac{2}{\Delta t} = 0$, with $\xi\equiv\{x_{Z_1}(t-\Delta t)-x_1\}\frac{2}{\Delta t} + \dot x_{Z_1}(t-\Delta t)-\dot x_2$;

$\eta\ \{-x_{Z_1}(t-\Delta t)+x_1\}\dot x_2\frac{2}{\Delta t} - \dot x_{Z_1}(t-\Delta t)\dot x_2$ and $\psi\frac{2}{\Delta t}\equiv(\dot y_{Z_1}-\dot y_1)(y_{Z_1}-y_2)\frac{2}{\Delta t}$

$$\text{With } \zeta\equiv\eta+\psi\frac{2}{\Delta t} \text{ one has: } \dot x_{Z_1}(t) = (-\xi+\sqrt{\xi^2-4\zeta})/2 \quad (3.2.2)$$

E_{kin} can be further found as above in 6.
If $\dot x_1$ and $\dot y_1$ are measured in (x_1,y_1) then, considering (x_1,y_1) and (x_{Z_1},y_{Z_1}):
$\dot\phi=(\dot x_1-\dot x_{Z_1})/(y_1-y_{Z_1})$ and $\dot\phi=(\dot y_1-\dot y_{Z_1})/(x_{Z_1}-x_1)$;(cf. AI-2 in Appendix I)

$$\text{Thus } \dot x_{Z_1} = \dot x_1-(y_1-y_{Z_1})(\dot y_1-\dot y_{Z_1})/(x_{Z_1}-x_1) \quad (3.3.1)$$

and the procedure after 3.2.1 can be followed again.
$\dot x_{Z_1}(t)^2+\dot x_{Z_1}(t)\xi+\eta+\psi\frac{2}{\Delta t} = 0$, with $\xi\equiv\{x_{Z_1}(t-\Delta t)-x_1\}\frac{2}{\Delta t} + \dot x_{Z_1}(t-\Delta t)-\dot x_1$;

$$\eta \equiv -\{x_{Z_1}(t)+x_1\}\dot{x}_1 \frac{2}{\Delta t} - \dot{x}_{Z_1}(t)\dot{x}_1 \quad \text{and} \quad \psi \frac{2}{\Delta t} \equiv \{\dot{y}_{Z_1}(t)-\dot{y}_1\}\{y_{Z_1}(t)-y_1\}\frac{2}{\Delta t}$$

$$\text{With } \zeta \equiv \eta + \psi\frac{2}{\Delta t} \text{ one has: } \dot{x}_{Z_1}(t) = (-\zeta \pm \sqrt{\zeta^2 - 4\zeta})/2 \qquad (3.3.2)$$

EXPERIMENTAL METHODS; DATA STORAGE AND PROCESSING

Recordings in time of the angular velocity and angle rotation and of the displacements in x- an y-direction of the centre of gravity of a specimen half, using a laser-Doppler technique.

The time independent relevant data of the specimens for the recordings in the performed tests are summarized in Table 1. The velocities v_1 and v_2 in x- and y-direction, or both in x-direction were measured in time with a laser-Doppler technique at these positions resp., cf. Appendix II (in Table 1 arrows indicate measuring direction). Scotch lite tape, type 3290 white, was glued onto the specimen surface to facilitate the observations. For storage of the v_1 and v_2 values with 5 µs intervals (one) Biomation 8100 and (four) Biomation 805 transient recorders were at disposal. The first one functions as "master" and triggers the other ones; it was externally triggered by an impact signal ("breaking wire") of projectile and specimen. The output of the straingauges responses on the supports was recorded in intervals of 5 µs by parallel channels (1 and 2) of the (Biomation 8100) transient recorder. Parallel channels 5 up to 6 of the (Biomation 805) transient recorder were used for the (v_1,v_2) recordings, applying the same time clock (set by crystal resonance frequency and providing the 5 µs interval signal storage.) The applied high speed camera was a moving film Hycam camera, model K20 S4W, provided with a rotating prism unit K20 HW and sectors shutter 1:5. This allows to record 10^4 f.p.s. with an illumination time of 1/5 x 10^{-4} sec. The objective was from Schneider with focal distance 3.5 mm; opening 1:2; applied was diafragma 8. Kodak Plus X 16 mm film with image dimensions 10 x 8 mm was used. Illumination proceeded in a continuous way by 6 halogen bulbs with reflector (each bulb 36 V - 340 watt.), which cast light on the specimen under 45°. The specimen was sprayed with "anti-reflex". The camera was used to trigger the electrical valve of the gasgun, which admits the compressed air in the barrel for driving out the projectile. The camera gives an opening signal to this valve ca. 0.1 sec. after start of the film rotation, which causes the projectile to hit the specimen some 500 ms later (of which ca. 100 ms are used for travel through the barrel of the projectile). At that time the rotating film speed of the camera (≈ 100 m/sec.) has become rather constant (this occurs after 70 to 100 m film is being spent). The pictures shot after this period start to show the projectile. From the velocity of the projectile - which is known from these pictures and also from the response of an illuminated photocell array onto which the passing projectile casts its shadow, cf. Van Elst (1) - and its distance to the specimen, the time at which the relevant picture is shot, is known. As light pulses with intervals of 1 ms are recorded on the film as well, the time clock of the film can thus be linked to that of the transient recorders. This allows to indicate the cracklength in the "read-out" of the transient recorders, which was processed with intervals of 50 µs for y_1 and y_2, the ordinates (in striker direction) of the fixed laboratory positions, where v_1 and v_2 were observed. With intervals of 25 µs the straingauges responses of the forces P_1 and P_2 on supports 1 and 2 resp. were read. These data allow to find the possible change of (translational) momentum of specimen in striker direction, the velocity in x-direction of the centre of gravity of a specimen half, its angular velocity, as elaborated by Van Elst and Lont (2) and the synchronous value of the cracklength. The velocities V_o and V of the projectile with mass M, just before and after impact with the specimen resp., measured with the

Table 1: Time independent data of performed tests

specimen code nr.	a_o [m]	m [kg]	M [kg]	V_o [ms^{-1}]	V [ms^{-1}] photocell	V [ms^{-1}] film	(x_1,y_1) [m]	(x_2,y_2) [m]	v_1	v_2
Fe510-nr. 3	0.050	8.6	5.89	81.7	16.6	- 16.6	(0.150, 0)	(0.170, 0)	ẏ ↑	ẋ ←
HY130-nr. 3	0.050	8.4	5.89	81.2	5.9	- 5.9	(0.150, 0) =	(0.150, 0)	ẏ ↑	ẋ ←
HY130-nr. 7	0.075	8.4	5.784	81.5	5.7	- 9.0	(0.150, 0) =	(0.150, 0)	ẏ ↑	ẋ ←
HY130-nr. 6	0.099	8.4	5.784	81.2	6.2	- 9.8	(0.150, 0)	(0.170, -0.010)	ẏ ↑	ẋ ←
Fe510-nr. 4	0.050	8.6	5.784	81.7	11.9	- 17.4	(0.180, 0)	(0.180, -0.040)	ẋ →	ẋ ←
HY130-nr. 8	0.075	8.4	5.784	82.4	6.7	- 10.6	(0.180, 0)	(0.180, -0.040)	ẋ →	ẋ ←
HY130-nr. 11	0.050	8.4	5.784	81.9	4.8		(0.180, 0)	(0.180, -0.040)	ẋ →	ẋ ←
HY130-nr. 9	0.025	8.4	5.784	82.8	0.9		(0.180, 0)	(0.180, -0.040)	ẋ →	ẋ ←
HY130-nr. 10	0.025	8.4	5.784	81.9	0.7	-(1.4?)	(0.180, 0)	(0.180, -0.040)	ẋ →	ẋ ←

Centre of gravity of (right) specimen half of Fe510 specimen (0.1125, 0) m

Centre of gravity of (right) specimen half of HY130 specimen (0.110, 0) m

N.B. Arrows indicate direction of measurement; stated values of v_1 and v_2 are "as-is", i.e. arrow indications are taken into account in these figures.

photocell array as described in Van Elst (1) are stored in the Biomation 850 transient recorder with 5 μs sampling time as well; these velocities could be compared with those deduced from the high speed photographic recordings. A manual calculator (Hewlett and Packard 97), which could be considered adequate for the data processing, was used.
It was assumed that the momentum transfer from projectile to specimen proceeded linearly in time and was accomplished in 250 μs; cf. 1.1. [This in fact appears somewhat better justified, if the specimen dimensions in striker direction (being 100 mm) would have been larger than the projectile length (being 600 mm) and the cross section of projectile and specimen rather the same. For such latter situation an (elastic) approximation of the transferred rectangular pulse time is $\tau = 2L/c = \frac{2x600mm}{5\ mm/\mu s} = 240\ \mu s$ with L = projectile length and c = sound velocity. The applied force $p_T/\tau \simeq \frac{1}{2}sc(V_o-V)$ with s = specific mass of specimen material is then constant for $p_T=M(V_o-V)$ = totally transferred momentum by projectile in time 2L/c. As during the first 250 μs no loss of contract was observed between projectile and specimen in the high speed photographic recordings of the performed tests, the mentioned assumption appears a fair approximation.]

RESULTS

The evaluation of $\frac{1}{2}m\dot{y}_{Z_1}^2$, $\frac{1}{2}m\dot{x}_{Z_1}^2$, $\frac{1}{2}T\dot{\phi}^2$ and ϕ for a specimen half at succesfully performed tests proceeded with a manual calculator, using the relevant algorithms as developed above (cf. also Appendix I). (The observed velocities in (x_1,y_1) and $x_2,y_2)$ and the calculated data outputs of $\dot{\phi}$, ϕ, $\dot{y}_{Z_1}$, y_{Z_1}, $\dot{x}_{Z_1}$, x_{Z_1} are collected in Van Elst and Lont (2), which can be obtained on request.) From the experiment on a specimen with nearly through initial ligament an estimate of the dissipated energy $E_{diss;p}$ by projectile penetration into the specimen only could be made. This latter energy dissipation presumably is completed before crack extension starts for finite ligament specimens. To find the energy dissipation $E_{diss;a}$ at crack extension the total energy dissipation $E_{diss} = \frac{1}{2}M(V_o^2-V^2)-E_{kin}$ has to be decreased with this $E_{diss;p}$. From the experiment 6 was estimated $E_{diss;p}$ = 6.5 kJ (however, cf. DISCUSSION). In Table 2 the crack extension in time for those tests where high speed photography was succesfully applied, is given.
Figures 4a and 4b show examples of the high speed photography recordings (16 consecutive relevant frames are presented). In Fig. 5 the totally dissipated energy for specimen separation E^{sep}_{diss} was plotted versus initial ligament ("multiple specimens approach"). Also $(E^{sep}_{diss} - E_{diss;p})/b(w-a_o$ was plotted versus $w-a_o$; this shows the anticipated linear behaviour {cf. Van Elst (3) and DISCUSSION}. Relevant numerical data are listed in Table 3. The dissipated energy $\frac{1}{2}M(V_o^2-V^2)-E_{kin}-E_{diss;p}$ and the cracklength a were plotted as functions of time. Examples are Figures 6a and 6b. From these diagrams also the diagrams of dissipated energy versus cracklength were plotted for the single test pieces; cf. DISCUSSION.

ANALYSIS OF EXPERIMENTAL RESULTS

A rather large scatter of the E_{kin}-evaluations in time, also in its components: $E_{transl} = 2 \times \frac{1}{2}m\dot{y}_{Z_1}^2$; $E_{vib} = 2 \times \frac{1}{2}m\dot{x}_{Z_1}^2$ and $E_{rot} = 2 \times \frac{1}{2}T\dot{\phi}^2$,

Table 2: High speed photographic recordings of extending crack in time.

	HY 130 nr. 8		HY 130 nr. 11		HY 130 nr. 9		HY 130 nr. 10		HY 130 nr. 3		HY 130 nr. 7		HY 130 nr. 6	
picture nr.	t [μs]	a [mm]	t [μs]	a [mm]	t [μs]	a [mm]	t [μs]	a [mm]	t [μs]	a [mm]	t [μs]	a [mm]	t [μs]	a [mm]
0								25.5						
1	100	75	31.3	49.0	25	24.8	104	25.5	50	46	50	75	60	99
2	203.4	75	134.7	50.0	129.2	25.7	208	25.5	153.4	46	152.6	75	162	
3	306.8	82.5	238.1	50.0	233.4	26.2	312	39.2	256.8	55	255.2	76	264	
4	410.2	91.3	341.5	68.6	337.6	45.6	416	55.9	360.2	74	357.8	86	366	
5	513.6	95.1	444.9	83.3	441.8	59.2	520	70.6	463.6	87	460.4	92	468	100
6	617.0	98.1	548.3	88.2	546.0	73.8	624	82.4	567.0	91	563.0	96	570	
7	720.4	99.0	651.7	91.7	650.2	83.5	728	86.3	670.4	93	665.6	97	672	
8	823.8	100	755.1	93.1	754.4	83.5	832	87.3	773.8	97	768.2	99	774	
9	927.2	100	858.5	95.1	858.6	92.2	936	91.2	877.2	98	870.8	100	876	
10	1030.6		961.9	96.6	926.8	93.7	1040	93.1	980.6	100	973.4	100	978	
11	1134.0		1065.3	98.0	1067.0	95.6	1144	96.1	1084.0	100	1076.0	100	1080	
12			1168.7	98.5	1171.2	96.6	1248	96.1	1187.4	100				
13					1275.4	97.6	1352	96.1						
14					1379.6		1456	97.1						
15					1483.8		1560	97.5						
16							1664	97.5						
17							1768	98.0						
18							1872	100.0						
19							1976							
20							2080							

HY130-nr. 8: $a - 75.0 = -21.91 + 1.24 \times 10^{-1}t - 8.19^5 \times 10^{-5}t^2$
HY130-nr. 11: $a - 50.0 = -67.92 + 3.82 \times 10^{-1}t - 4.31 \times 10^{-4}t^2 + 1.63 \times 10^{-7}t^3$
HY130-nr. 9: $a - 25.0 = -59.74 + 3.18 \times 10^{-1}t - 2.64 \times 10^{-4}t^2 + 7.55 \times 10^{-8}t^3$
HY130-nr. 10: $a - 25.5 = -47.83 + 2.63 \times 10^{-1}t - 1.93 \times 10^{-4}t^2 + 4.67^5 \times 10^{-8}t^3$
HY130-nr. 3: $a - 46 = -79.24 + 4.87 \times 10^{-1}t - 6.24 \times 10^{-4}t^2 + 2.72 \times 10^{-7}t^3$
HY130-nr. 7: $a - 75 = -46.11 + 2.62 \times 10^{-1}t - 3.41 \times 10^{-4}t^2 + 1.54 \times 10^{-7}t^3$

} a in mm; t in μs

was found. This is probably due to the non equilibrium stress configuration at each moment in the impacted tearing specimen. This will deviate from the static one for a certain deflection not only by (possible) stress amplitude (increase) due to dynamic effects, but also by the presence of running stress waves. The laser-Doppler technique measures the therefore relevant displacement velocities at the specimen surface. However when the movement of the specimen is very fast (as in the experiments on specimens with practically zero ligament) the available laser-Doppler technique equipment can obviously not follow, when the acceleration is too fast. A frequency of 40 kH per ms^{-1} is observed by this equipment (cf. Appendix II). The maximum frequency change per unit time that can be observed is 5Mhz per millisecond.

This implies, that accelerations up to $1.25 \times 10^5\ ms^{-2} \simeq 12500$ g can be followed. If a particle velocity of $\dot{u} = 25\ ms^{-1}$, corresponding with an (elastic) stress of $sc\dot{u} = 8 \times 10^3 \times 5 \times 10^3 \times 25\ Nm^{-2} = 1000\ MNm^{-2}$, is achieved in 10 μs, the acceleration is of the order $25 \times 10^5\ ms^{-2}$, which is 20 x larger. Running stress waves can thus imply errors of velocity recordings in time, while moreover the geometrical link between velocities in different points as illustrated in Fig. 3 can be violated. The applied interpretation of the velocities as recorded by the laser-Doppler technique can then be at fault. Also a non symmetrical division of the specimen by the moving crack will entail unequal distribution of kinetic energies in both specimen halves; as only one specimen half was observed this too accounts for scatter. [An analytical estimate of the kinetic energy obtained by a specimen with zero ligament can in principle be given as well. For this a specimen with zero ligament, but with an ideal hinge at the point of impact, operative after impact as long as it experiences compressive forces and then moving in striker direction can be considered. The relevant differential equations describing the movement of such a specimen are given by Van Elst and Lont (2). These equations suggest that the rotational movement has a harmonic character with a damping proportional to $\dot{\phi}^2$; it might account for the oscillatory appearance of $\frac{1}{2}T\dot{\phi}^2$ as calculated; a frequency estimate has not yet been made.]

The totally dissipated energies E^{sep}_{diss} for separation of the specimens:

$E^{sep}_{diss} = \frac{1}{2}m(V_o^{\ 2} - V^2) - E^{sep}_{kin}$, as summarised in Table 3 and plotted versus $(w-a_o)$ in Fig. 5 (cf. RESULTS), were curve fitted according to:

$$E^{sep}_{diss;a} = E^{sep}_{diss} - E_{diss;p} = \bar{R}b(w-a_o) + \bar{S}b(w-a_o)^2 \qquad (8)$$

with presumably $\bar{R}$ = average fracture resistance with the dimensions (MNm^{-1}) of an effective surface energy and $\bar{S}$ = effective energy density with the dimensions $[MNm^{-2}]$. Such a description was found adequate in tearing experiments on notched specimens of other (ductile) steels (in particular line pipe steel), when a completely yielding ligament occurs; cf. Van Elst (3). $\bar{R}$ refers to the local plastic work in the so called process zone near the crack tip; while $\bar{S}$ refers to remote global plastic work unavoidably accompanying the tearing. As figures were obtained:

$$E_{diss;p} = 3.90\ kJ;\ \bar{R} = 1.18\ MNm^{-1};\ \bar{S} = 21.6\ MNm^{-2};\ \gamma^2 = 0.894.$$

In this description the dissipated energy value estimated from the experiment with nearly through ligament (HY130-nr. 6) was rejected, as this would have implied a minimum energy dissipation for finite ligament (and a negative value of $\bar{R}$). However from the model with zero ligament as analysed by Van Elst and Lont (2) a satisfactory value for this dissipated energy was found, viz. 4.1 kJ. Using the assumption that the momentum transfer from projectile to specimen during impact linearly proceeds in time (cf. 1.1), the kinetic

Table 3: Dissipated energy for separation of specimens

specimen	a_o [m]	$\frac{1}{2}M(V_o^{\ 2}-V^2)$ [kJ]	E^{sep}_{kin} [kJ]	E^{sep}_{diss} [kJ]	$E^{sep}_{diss;a}$ * [kJ]
HY130-nr. 7	0.075	19.12	13.0	6.1	2.2
HY130-nr. 8	0.075	19.51	13.5	6.0	2.1
HY130-nr. 3	0.045	19.32	9.5	9.8	5.9
HY130-nr. 11	0.050	19.33	10.0	9.3	5.4
HY130-nr. 9	0.025	19.83	4.7	15.1	11.2
HY130-nr. 10	0.025	19.40	4.1	15.3	11.4
HY130-nr. 6	0.099	18.96	12.9	6.0(?)	2.1
Fe510-nr. 3	0.050	18.55	8.5	10.0	6.1
Fe510-nr. 4	0.050	18.89	11.0	7.9	4.0

(* Assumedly $E_{diss;p}$ = 3.90 [kJ])

Table 4: Estimated $\tilde{R}$-values from single SENB impact test evaluation of dissipated energy, as a function of cracklength (for relevant crack velocity)

specimen	a_o [m]	$\simeq \tilde{R}$ $[MNm^{-1}]$	$\simeq \bar{\dot{a}}$ $[ms^{-1}]$	interval [μs]
HY130-nr. 3	0.045	1.0	160	250 - 500
HY130-nr. 11	0.050	1.50	170	250 - 450
HY130-nr. 10	0.025	1.80	137.5	200 - 600
HY130-nr. 6	0.099	-	-	-
HY130-nr. 8	0.075	0.96	62.5	200 - 550
HY130-nr. 7	0.075	1.4 (-2?)	67	250 - 600
HY130-nr. 9	0.025	1.29	167	250 - 550
Fe510-nr. 4	0.050	0.8 (?)	175	150 - 350
Fe510-nr. 3	0.050	1.1	160	250 - 550

energy shows a monotonic ("smooth") increase. Crack extension starts at about the time that this momentum transfer has been completed (presumably after ca. 250 μs). From this onwards the kinetic energy as deduced from the velocity recordings with the laser-Doppler technique shows an oscillatory behaviour. Consequently the anticipated decrease of kinetic energy when the crack extends is not easily detected and in fact it even seems sometimes absent. $E_{diss;a} = \frac{1}{2}M(V_o^2 - V^2) - E_{diss;p} - E_{kin}$ was plotted versus time. Figures 6a and 6b show examples; on the same time axis the cracklength a is plotted. This allows to find the diagram of $E_{diss;a}$ versus a (in which the oscillatory behaviour of the kinetic energy of the specimen effectuates less disturbance). The estimate of the slope in a relevant a-interval, usually (a_o,w) in this latter diagram offers a R-value, indicated as $\tilde{R}$. These $\tilde{R}$-values are presented in Table 4 together with the estimated average crack velocity values $\dot{a}$ (in the considered time intervala). A (systematic) error in $E_{diss;p}$ will not influence values of $R = \frac{dE_{diss;a}}{da}$ or its approximation $\tilde{R}$. [The intermittent drawn part of the curve $E_{diss;a}$ in the time interval (0-150 μs) was obtained by assuming that the kinetic energy loss of the projectile and energy dissipation by projectile penetration into the specimen linearly proceeded in time. A possible physical meaning of this $E_{diss;a}$ before crack extension starts might be attributed to a dissipation of energy required for crack initiation.]

J AND R INTERPRETATION OF RESULTS FROM LIMIT CONDITIONS

Though for the dynamic non equilibrium situation the J-integral is path dependent, yet a quasi-static J-integral evaluation was explored. As load data causing specimen deflection are not (directly) observable - in fact deflection and tearing proceed, when the specimen is free from external loads or moments after impact - an expression for J in the observable ϕ is required. Assumedly the beyond limit load situation is realized already at initiation and using the relevant expression for 3 points SENB-specimen for this, cf. e.g. Rice, Paris and Merkle (4), one derives with Q referring to the moment part causing deformation only:

$$J = \frac{Q\phi_{crack}}{b(w-a)}\{2 - \frac{(\phi_{crack})_{lim}}{\phi_{crack}}(1-16\beta D_2^{\,2})\} \qquad (9.1)$$

$$= D_2\bar{Y}w(1-\lambda)\phi_{crack}\{2 - \frac{(\phi_{crack})_{lim}}{\phi_{crack}}(1-16\beta D_2^{\,2})\} \qquad (9.2)$$

ϕ_{crack} = rotation angle, due to the crack; $\bar{Y}$ = effective yield strength; D_2=0.36, cf. Green and Hundy (5); $\beta = \frac{1}{2\pi}$ for the assumedly relevant plane stress situation; $16\beta D_2^{\,2}$ = 0.35 and can become up to 3 x smaller, when plane strain is prevailing. For $(\phi_{crack})_{lim}$ was taken ϕ at 250 μs; at this time initiation (usually) starts an the limit load situation is arrived at (cf. N.B.).

In Table 5 thus evaluated J-values are presented. No correction for strain hardening was attempted, which unfavorably interferes with tearing modulus estimates from J/Δa-curves; cf. Fig. 7.

N.B. Up to limit load with $K^2 = \frac{16Q^2}{b^2(w-a^*)^3}$, cf. Wilson (6),

$$\phi_{crack} = \frac{b}{E}\int_o^a \frac{\partial K^2}{\partial Q}\,da^* = \frac{16Q}{Eb(w-a^*)^2}, \text{ cf. Rice, Paris and Merkle (4),}$$

and with $r_Y = \frac{\beta K^2}{Y^2}$ and $a^* = a + r_Y$ one has:

$$Q = \frac{\phi_{crack}Eb(w-a^*)^2}{16} = \frac{\phi_{crack}Eb(w-a)^2}{16}\{1 - \frac{\beta K^2}{Y^2(w-a)}\}^2 \qquad (10.1)$$

As $K^2 = \frac{16Q^2}{b^2(w-a^*)^3} = E^2\frac{(w-a^*)}{16}\phi_{crack}^{\,2}$, also

$$Q = \frac{\phi_{crack}Eb(w-a)^2}{16}\{1 - \frac{\beta}{16}(\frac{\phi_{crack}}{\varepsilon_Y})^2\}^2 \quad \text{with } \varepsilon_Y = \frac{Y}{E} \qquad (10.2)$$

$$J = \frac{2Q\phi_{crack}}{b(w-a)}[1 - \tfrac{1}{2}\{1 - \frac{\beta}{16}(\frac{\phi}{\varepsilon_Y})^2\}] \qquad (11.1)$$

$$J = \frac{2E(w-a)}{16}\phi_{crack}^{\,2}[\{1 - \frac{\beta}{16}(\frac{\phi_{crack}}{\varepsilon_Y})^2\}^2 - \tfrac{1}{2}\{1 - \frac{\beta}{16}(\frac{\phi_{crack}}{\varepsilon_Y})^2\}^3] \qquad (11.2)$$

Completely yielding ligament is then estimated at $\phi \simeq \frac{4}{\sqrt{\beta}}\varepsilon_Y \simeq 4\sqrt{2\pi}\,\varepsilon_Y \simeq 10\varepsilon_Y$ (for plane stress) and this indeed is achieved after ≃ 250 μs (it is not meant to say that initiation and limit load always coincide).

To account for the absorbed energy during crack extension in SENB-specimens under limit load conditions one has with:

$$P_{lim}(\lambda) = \frac{4}{3}\bar{Y}b(w-a)^2/2\ell = \frac{4}{3}\bar{Y}bw^2(1-\lambda)^2/2\ell \qquad (12)$$

and thus for span $2\ell = 4w$ as relevant: $P_{lim} = \frac{1}{3}\bar{Y}bw(1-\lambda)^2$

$$E(\lambda,\lambda_o) = \frac{1}{3}\bar{Y}bw\int_{a_o}^{a}(1-\lambda)^2 df = \frac{1}{3}\bar{Y}bw^2\int_{\lambda_o}^{\lambda}(1-\lambda)^2\frac{\dot{f}}{\dot{a}}d\lambda = \frac{1}{9}\bar{Y}bw^2\frac{\bar{\dot{f}}}{\bar{\dot{a}}}\{(1-\lambda_o)^3 - (1-\lambda)^3\} \qquad (13)$$

$$E^{sep}_{diss}(\lambda,\lambda_o) = \lim_{\lambda\to 1} E(\lambda,\lambda_o) = \frac{1}{9}\bar{Y}bw^2\frac{\bar{\dot{f}}}{\bar{\dot{a}}}(1-\lambda_o)^3 \qquad (14)$$

With $\bar{Y}$ = 900 MNm^{-2}; b = 0.05 m; w = 0.1 m and - according to observation - $\dot{f} \simeq \dot{y}_{Z_1}$ = 25 ms^{-1}; $\dot{a}$ = 100 ms^{-1}; $\frac{1}{9}\bar{Y}bw^2\frac{\dot{f}}{\dot{a}}$ = 0.0125 MNm, 14 appears to offer a rather satisfactory description of $E^{sep}_{diss} - E_{diss.p}$, while 13 describes $\frac{1}{2}M(V_o^{\,2} - V^2) - E_{kin} - E_{diss.p}$; cf. Figures 5 and 6a and 6b with Fig. 8.

$$R(\lambda) = \frac{1}{bw}\frac{dE}{d\lambda}(\lambda,\lambda_o) = \frac{P_{lim}(\lambda)}{b}\frac{\bar{\dot{f}}}{\bar{\dot{a}}} = 7.5(1-\lambda)^2 MNm^{-1} \text{ and } \tilde{R} = \frac{1}{9}\bar{Y}w\frac{\bar{\dot{f}}}{\bar{\dot{a}}}(1-\lambda_o)^2$$

CONCLUSIONS

Displacement controlled impact tests on SENB-specimens, in which contact between striker and specimen and supports and specimen is lost, nevertheless allow estimates of J_{Ic}, J/Δa-curve and dissipated energy E(a) by suitable

Table 5: J-estimates for HY130 steel in SENB high velocity impact tests from deflection angles (calculated) with observed specimen surface velocities and (in time curve fitted observed) crack length values, using (24.2). Tearing modulus estimates from in time curve fitted J-values and using $\frac{dJ}{da} = \dot{J}/\dot{a}$.

specimen code nr.	t [ms]	a [mm]	ϕ x10^3	J/D_2Yw	J $[MNm^{-1}]$	$\dot{J}$ $[MNm^{-1}s^{-1}]$	$\dot{a}$ $[ms^{-1}]$	$\frac{dJ}{da}$ $[MNm^{-2}]$	$\frac{E}{Y^2}\frac{dJ}{da}$
HY130-nr.10	250	32.09	38.1	0.0349	0.818	6940	175	(40)	(9.8)
a_o=25.5 mm	300	40.46	51.3	0.0463	1.084	4140	159	26	6.4
	350	48.08	62.1	0.0516	1.208	1340	145	9	2
	400	54.98	77.0	0.0582	1.361		131		
	450	61.20	95.5	0.0645	1.509		118		
	($J = -2.642 + 0.02094\ t - 0.000028\ t^2$ door t = 250, 300, 350 μs resp.)								
HY130-nr. 9	250	29.44	34.7	0.0331	0.773	6790	200	(34)	(8.4)
a_o=25.0 mm	300	38.94	46.8	0.0434	1.015	2890	180	16	4.
	350	47.46	54.5	0.0454	1.062	-1010?	161		
	400	55.05	66.1	0.0493	1.153		143		
	450	61.78	73.8	0.0478	1.118		126		
	($J = -3.362 + 0.02629\ t - 0.000039\ t^2$ door t = 250, 300, 350 μs resp.)								
HY130-nr.11	250	53.19	53.9	0.0341	0.797	5460	197	(28)	(6.9)
a_o=50.0 mm	300	62.29	75.2	0.0435	1.018	3160	167	19	4.7
	350	69.97	97.6	0.0481	1.125	-1010?	140		
	400	76.95	113.9	0.0443	1.040		115		
	450	81.56	121.6	0.0384	0.898		93		
	($J = -2.018 + 0.01696\ t - 0.000023\ t^2$ door t = 250, 300, 350 μs resp.)								
HY130-nr. 3	250	53.76	27.3	0.0170	0.399	5110	226	(23)	(5.7)
a_o=46.0 mm	300	64.04	43.6	0.0250	0.584	1310	186	7	1.7
	350	72.43	58.3	0.0273	0.638	-90?	150		
	400	79.13	72.7	0.0266	0.623		118		
	450	84.34	86.7	0.0244	0.570		91		
	($J = -2.491 + 0.01811\ t - 0.000026\ t^2$ door t = 250, 300, 350 μs resp.)								
HY130-nr. 7	250	75.48	53.0	0.0175	0.411	2510	120	(21)	(5.2)
a_o=75.0 mm	300	80.96	73.4	0.0214	0.501	1310	99	13	3.2_5
	350	85.42	94.9	0.0227	0.530	110	80	1	0.2
	400	88.99	114.7	0.0215	0.502		63		
	450	91.77	133.6	0.0152	0.448		49		
	($J = -0.954 + 0.00851\ t - 0.000012\ t^2$ door t = 250, 300, 350 μs resp.)								
HY130-nr. 8	250	78.97	36.9	0.0105	0.245	1930	83	(23)	(5.7)
a_o=75.0 mm	300	82.91	50.2	0.0131	0.306	730	75	10	2.5
	350	86.45	60.8	0.0132	0.306		67		
	400	89.58	71.6	0.0149	0.348		58		
	450	92.30	84.4	0.0112	0.261		50		
	($J = -0.975 + 0.00793\ t - 0.000012\ t^2$ door t = 250, 300, 350 μs resp.)								

recordings of displacement, velocity, angular velocity and cracklength in time.
In the investigated upper shelf level, where presumably ductility dictated limit (dynamic) moment conditons, J-values appear to remain ligament dependent, while the dissipated energy for crack extension appears to be describable as: $E_{diss}(\lambda,\lambda_o) = \frac{1}{9}\{\bar{Y}b\bar{w}^2 f/\bar{\dot{a}}\}\Gamma(\lambda)$, with $\bar{Y}$ a yield strength value for relevant strainhardening and deformation rate and $\Gamma(\lambda)$ a geometrical factor as described in 13 and for $\lambda = w$ in 14 resp.

ACKNOWLEDGEMENTS

The larger part of this work was made possible by contract N68171-82-C-9517 with U.S.-Navy, to which our thanks are due for permission to publish this paper. The experimental work proceeded under guidance of Mr. M. Lont.

REFERENCES

1. Elst, H.C. van., Proc. of the 5th Int. Conf. on Fracture, ICF5, Cannes, France, 2, 1059-1072, 1981. (editor C. François at Pergamon Press).

2. Elst, H.C. van, and Lont, M.A., Metal Research Institute report 83M/42/0771-III/ELS-MC.

3. Elst, H.C. van, Proc. of the 4th AGA-EPRG Linepipe Research Seminar, I-nr. 7, 1981. (edited by G. Vogt at Mannesmann Forschungsinstitut, Duisburg, W-Germany).

4. Rice, J.R., Paris, P.C. and Merkle, J.G. Progress in flaw growth and fracture toughness testing. ASTM-STP 536, 231-245, 1973

5. Green, A.P. and Hundy, B.B., J. of Mech. and Phys. of Sol. 4, 128-144, 1956.

6. Wilson, W.K., J. of Eng. Fracture Mech. 2 nr. 2, 169-171, 1970.

7. Oldengarn, J. Prabha Venkatesh, J. Phys. E. Sci. Instr. 9, 1009-1012, 1976.

8. Oldengarn, J., Opt. and Laser Techn. 9, 69-71, 1977.

KEYWORDS

Dynamic fracture propagation resistance; high velocity impact; gasgun high speed photography; laser-Doppler technique; electronic instrumentation; straingauges; photocell; energy and momentum balance; energy dissipation; crack velocity; J-integral; limit load and moment; SENB-specimen.

SYMBOLS

x,y,z = Cartesian coördinates of to the laboratory fixed (Euler) OXYZ-system
O = centre of initial rest position of specimen
OX = length direction of initial rest position of specimen
OY = height direction of initial rest position of specimen opposite to crack extension direction in OXYZ
OZ = thickness direction of (initial rest position) of specimen
$\underline{x},\underline{y},\underline{z}$ = Cartesian coördinates of to the moving specimen half 1 fixed (Lagrange) $\underline{OXYZ}$-system

$\underline{0}$	= to a specimen half fixed point, coinciding with 0 in the initial rest position	
$\underline{OX}$	= length direction of moving specimen half 1 rotating in right hand way in YOX-plane	
$\underline{OY}$	= height direction of moving specimen half 1	
$\underline{OZ}$	= thickness direction of (moving) specimen half	
t	= time	s
ℓ	= length of specimen half	m
2ℓ-2q	= span of specimen	m
w	= height (or width) of specimen	m
b	= thickness of specimen	m
D	= diameter supports	m
m	= mass of specimen half	kg
s	= density of specimen material	kg m^{-3}
a	= cracklength	m
T	= moment of inertia of specimen half w.r.t. axis in thickness direction through its centre of gravity	kg m^2
φ	= rotation angle	
ρ	= rotation factor	
M	= mass of projectile	kg
V	= projectile velocity (in OXYZ-system)	ms^{-1}
r	= polar radius	m
p	= momentum	kg ms^{-1}
v	= velocity in surface point of impacted specimen	ms^{-1}
ρ	= rotation factor = $(a_e-a)/(w-a)$	
P	= force	N
τ	= impact duration	s
f	= deflection	m
δ	= crack mouth edges distance	m
CTOD	= crack tip opening displacement	m
C	= elastic compliance	mN^{-1}
E	= energy	J
E	= Young's modulus	MNm^{-2}
R	= fracture resistance	Nm^{-1}
Y	= yield strength	MNm^{-2}
Q	= applied moment	Nm
I	= area moment of inertia of cross section	m^{-1}
c	= sound velocity	ms^{-1}
γ	= correlation coëfficient for curve fitting	
J	= J-integral	MNm^{-1}
λ	= a/w	

subscript:	to:	
1,2	1,m,T,p,Z,v	specimen half 1,2
o	a,V,δ	initial value
i	t,φ,ρ,a	moment of impact of specimen and supports
e	a	elastic equivalent
Z	x,r	centre of gravity
p	τ,P	projectile and specimen
s	τ,P	support(s) and specimen (half)
kin	E	kinetic energy
transl	E	translational kinetic energy
vib	E	vibrational kinetic energy
rot	E	rotational kinetic energy
elast	E	elastic energy
diss	E	dissipated energy
diss; p	E	dissipated energy for ligament zero (dissipated energy due to penetration of projectile into specimen)
diss; a	E	dissipated energy by crack extension

lim	φ,Q,P	limit load or moment conditons
Y	r	plastic zone size at crack tip
superscript:	to:	refers to:
sep	E	at complete specimen separation
*	a	notional cracklength ($a^* = a+r_y$)

abbreviations: SENB, single edge notch bend; h.s.p.(r.), high speed photography (recordings); f.p.s., frames per second

APPENDIX I. KINEMATIC DESCRIPTION OF IMPACTED SENB-SPECIMEN

OXYZ is the to the laboratory fixed Cartesian (Euler) system with the orgin in the original centre position of the specimen and OX is the length direction, OY is the height direction, OZ is the thickness direction. (span = 2ℓ-2q; height = w; thickness = b)
$\underline{OXYZ}$ is the to the moving specimen half 1 fixed Cartesian (Lagrange) system with the origing $\underline{0}$ in the centre of the specimen half bounding plane (height x thickness) containing an initial notch plane and OX in the length direction. $\underline{OX}$ rotates in right hand direction in the XOY-plane, if the specimen is impacted in x = 0, y = $\frac{w}{2}$, $-\frac{1}{2}b \leq z \leq \frac{1}{2}b$ at t = 0. (cf. Fig. 2).

The transformation relations between the coordinates of the laboratory system OXYZ and the to specimen half 1 fixed system $\underline{OXYZ}$ (cf. Fig. 2) read:

$$x-x_o = \underline{x}\cos\phi + \underline{y}\sin\phi;\ y-y_o = -\underline{x}\sin\phi + \underline{y}\cos\phi \qquad \text{(AI-1.1)}$$

$$\underline{x} = (x-x_o)\cos\phi - (y-y_o)\sin\phi;\ \underline{y} = (x-x_o)\sin\phi + (y-y_o)\cos\phi \qquad \text{(AI-1.2)}$$

with $\underline{0} = (\underline{o},\underline{o}) = (x_o,y_o)$ (and φ taken as positive for right hand turning)

For a fixed point $(\underline{x},\underline{y})$ of the specimen half:

$$\dot{x}-\dot{x}_o=(-\underline{x}\sin\phi + \underline{y}\cos\phi)\dot{\phi}=(y-y_o)\dot{\phi};\ \dot{y}-\dot{y}_o = (-\underline{x}\cos\phi-\underline{y}\sin\phi)\dot{\phi} = -(x-x_o)\dot{\phi} \qquad \text{(AI-2)}$$

$$\dot{\phi} = (\dot{x}_1-\dot{x}_2)/(y_1-y_2)\ ;\ \dot{\phi} = (\dot{y}_3-\dot{y}_4)/(x_4-x_3), \qquad \text{(AI-3)}$$

If $\dot{x}_1$ and x_2 are measured in (x_1,y_1) and (x_2,y_2) and $\dot{y}_3$ and $\dot{y}_4$ are measured in (x_3,y_3) and (x_4,y_4) resp. Considering Fig. 3:

$$\dot{x}=o \text{ implies } y_{\dot{x}=o}=y_o-\dot{x}_o/\dot{\phi};\ \dot{y}=o \text{ implies } x_{\dot{y}=o}=x_o+y_o/\dot{\phi} \qquad \text{(AI-4.1)}$$

The "pole" Q of the Euler system OXY is: $Q = \{x_o+\dot{y}_o/\dot{\phi},\ y_o-\dot{x}_o/\dot{\phi}\}$ (AI-4.2)

If $\dot{x}_1$ and $\dot{x}_2$ are measured in (x_1,y_1) and (x_2,y_2) resp. then:

$$\dot{x}_2/\dot{x}_1 = (y_2-y_{\dot{x}=o})/(y_1-y_{\dot{x}=o}),\ \text{thus: } y_{\dot{x}=o}=(\dot{x}_1y_2-\dot{x}_2y_1)/(\dot{x}_1-\dot{x}_2) \qquad \text{(AI-5.1)}$$

If $\dot{y}_3$ and $\dot{y}_4$ are measured in (x_3,y_3) and (x_4,y_4) resp. then:

$$\dot{y}_4/\dot{y}_3 = (x_4-x_{\dot{y}=o})/(x_3-x_{\dot{y}=o}),\ \text{thus: } x_{\dot{y}=o} = (x_4\dot{y}_3-x_3\dot{y}_4)/(\dot{y}_3-\dot{y}_4) \qquad \text{(AI-5.2)}$$

Generally $\dot{x}=\{\dot{x}_1(y-y_2)-\dot{x}_2(y-y_1)\}/(y_1-y_2)$;

$$\dot{y}=\{\dot{y}_3(x-x_4)-\dot{y}_4(x-x_3)\}/(x_3-x_4) \qquad \text{(AI-6)}$$

For the rotation centre P of the (crack edges of the) specimen, one will have $x_P=0$; $\dot{x}_P=0$. (if the crack extends in the initial notch direction for which x=o). $P(\underline{o},\underline{y}_P) = P(o,y_P)$. (1.2) and (4.1) resp. offer:

$$y_P = -x_o\cos\phi/\sin\phi + y_o \text{ and } y_P = y_o - \dot{x}_o/\dot{\phi} \qquad \text{(AI-7)}$$

y_P is further given by (AI-5.1)

$$\text{From this: } \frac{\dot{x}_o}{x_o} = \frac{\cos\phi.\dot{\phi}}{\sin\phi};\ x_o = A\sin\phi \text{ and: } \underline{y}_P = -A \qquad \text{(AI-8.1)}$$

The rotation centre P of the impacted, moving and tearing specimen is located at a distance $\rho(w-a)$ before the crack tipand one will have (cf. Fig. 2):

$$A = a+\rho(w-a)-w/2 = a_e-w/2;\ \delta/2 = x_o a_e/(a_e-w/2) = a_e\sin\phi;$$

$$\text{CTOD} \simeq \delta(a_e-a)/a_e \simeq \delta-2a\sin\phi \qquad \text{(AI-8.2)}$$

In these considerations up to now $A=a+\rho(w-a)-w/2=a_e-w/2$ was constant, as a=constant. The model can be extended with a increasing to w and thus $A=a_e-w/2$ becoming zero for $a_e=w$ and $A<o$ for $a_e>w/2$. Note that $x_o(t^*)$ becomes then equal to $x_o(0) = 0$ for $a_e(t^*) = w/2$.

With the rotation centre P of the impacted, moving and tearing specimen located at a distance $(\rho(w-a)$ before the cracktip, cf. AI-8.2 one concludes from Fig. 2:

$$\{a+\rho(w-a)-w/2\}^2 = (a_e-w/2)^2 = (y_P-y_{Z_1})^2 + x_{Z_1}^2-(\ell/2)^2 \qquad \text{(AI-9.1)}$$

$$\underline{O}(\underline{o},\underline{o}) = \underline{O}(x_o,y_o) = \{(a_e-w/2)\sin\phi,\ y_{Z_1}+\frac{\ell}{2}\sin\phi\}$$

$a_e \equiv a+\rho(w-a)$ is thus known from AI-9.1 as y_P is given by AI-5.1 ;
y_{Z_1} follows from 2, while x_{Z_1} follows from 7.

When from high speed photographic recordings $a = a(t)$ {and (or) ϕ and $\frac{\delta}{2} = a_e\phi\}$ is known, then $\rho = \rho(a)$ is known.

For the moment of impact at $t = t_i$ of specimen and supports, the contact point $C(\underline{x}_c,\underline{y}_c) = C(x_c,y_c)$ will satisfy (cf. Fig. 2):

$$\underline{x}_c=\ell-q-(D/2)\phi;\ x_c=\ell-q-(D/2)\sin\phi_i = x_o+\{\ell-q-(D/2)\phi_i\}\cos\phi_i+(w/2)\sin\phi_i \qquad \text{(AI-10.1)}$$

$$\underline{y}_c=w/2;\ y_c=w/2+(D/2)(1-\cos\phi_i)=y_o-\{\ell-q-(D/2)\phi_i\}\sin\phi_i+(w/2)\cos\phi_i \qquad \text{(AI-10.2)}$$

N.B. For t=0 is $\underline{x}_c(o)=x_c(o)=\ell-q;\ \underline{y}_c(o)=y_c(o)=w/2$.

$$y_o=y_{Z_1}+(\ell/2)\sin\phi;\ x_o=\{a+\rho(w-a)-w/2\}\sin\phi=(a_e-w/2)\sin\phi \qquad \text{(AI-11)}$$

AI-10.1 and AI-11 offer:

$$\ell-q-(D/2)\sin\phi_i-(a_{ei}-w/2)\sin\phi_i = \{\ell-q-(D/2)\phi_i\}\cos\phi_i+(w/2)\sin\phi_i \qquad \text{(AI-12.1)}$$

AI-10.2 and AI-11 offer:

$$w/2+(D/2)(1-\cos\phi_i)-\{y_{Z_1}+\ell/2)\sin\phi_i\}=\{\ell-q-(D/2)\phi_i\}\sin\phi_i+(w/2)\cos\phi_i \qquad \text{(AI-12.2)}$$

The angle ϕ_i and $a_i+\rho_i(w-a_i) = \frac{1}{2}\delta_i/\phi_i$ at the moment $t = t_i$ can be found independently from high speed photography (in principle). The comparison with the solutions of these from AI-12.1 and AI-12.2 resp. appears a usuful monitoring for the integration procedures 2 and 6 resp.
It is noted, that from AI-1, using AI-11 generally:

$$x=(a_e-w/2)\sin\phi+\underline{x}\cos\phi+\underline{y}\sin\phi;\ y=y_{Z_1}+(\ell/2)\sin\phi-\underline{x}\sin\phi+\underline{y}\cos\phi \qquad \text{(AI-13.1)}$$

$$\dot{x}=\dot{a}_e\sin\phi+(a_e-w/2)\cos\phi.\dot{\phi}-\{y-y_{Z_1}-(\ell/2)\sin\phi\}\dot{\phi};$$

$$\dot{y}=\dot{y}_{Z_1}+(\ell/2)\cos\phi.\dot{\phi}-\{x-(a_e-w/2)\sin\phi\}\dot{\phi} \qquad \text{(AI-13.2)}$$

Note that from AI-13.1 and AI-13.2, cf. also Fig. 1,

$$x_{Z_1}=a_e\sin\phi-(w/2)\sin\phi+(\ell/2)\cos\phi;$$

$$\dot{x}_{Z_1}=\dot{a}_e\sin\phi+\{a_e\cos\phi-(w/2)\cos\phi-(\ell/2)\sin\phi\}\dot{\phi} \qquad \text{(AI-14)}$$

ϕ and a_e (also $\dot{\phi}$ and $\dot{a}_e$) can be found directly from h.s.p. recordings and thus x_{Z_1} (also $\dot{x}_{Z_1}$). But ρ - and thus a_e - estimates and thus x_{Z_1} will have poor accuracy.

APPENDIX II. PRINCIPLE OF LASER-DOPPLER TECHNIQUE

A particle moving with a velocity $\vec{u}_1$ into the directon of a light source emitting light with frequency ν_o (and wave length λ) will reflect light into all directions with a frequency $\nu_1 = \nu_o + + u_1/\lambda$. (Combination of Huygens and Doppler principle.) Let the particle be illuminated by two coherent light beams I and II, enclosing an angle 2i of which the bissectrix makes an angle α with the particle velocity $\vec{u}$ (i is small, $\alpha = \frac{\pi}{2}$). It can be noted that the frequency shift for light from beam I and II as reflected by the particle will be: $-\frac{u_1}{\lambda} = \frac{u}{\lambda}\cos(\alpha+i)$ and $+\frac{u_2}{\lambda} = \frac{u}{\lambda}\cos(\alpha-i)$ resp. A suitable photodiode will only detect light with a frequency ν_D equal to the difference between the frequencies of the by the particle reflected coherent interfering beams I and II. Referring to the relevant superposition of beam I and II (cf. Fig. AII-1):

$$\nu_D = \frac{u}{\lambda}\{\cos(\alpha-i)-\cos(\alpha+i)\} = \frac{2u}{\lambda}\sin\alpha\sin i \simeq \frac{2u}{\lambda}i(1-\frac{\beta^2}{2}\ldots)$$

$\beta = \frac{\pi}{2}-\alpha$ is the angle between the bissectrix of the angle 2i enclosed by the light beams I and II and the normal to the plane in which the particle moves, this plane being transversal to the plane of the light beams. Thus also:

$$\nu_D = \frac{u}{\lambda}\{-\sin(\beta-i)+\sin(\beta+i)\} = \frac{2u}{\lambda}\sin i\cos\beta \simeq \frac{2u}{\lambda}i(1-\frac{\beta^2}{2}\ldots);$$ cf. Oldengarn (7,8).

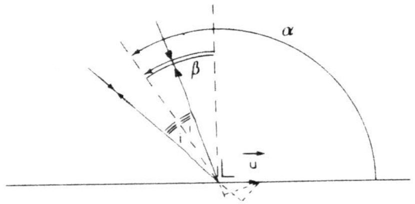

Fig. AII-1. Principle of laser-Doppler technique

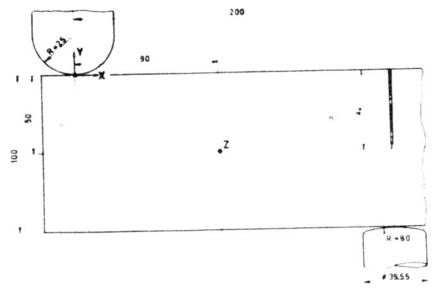

Fig. 1. SENB-specimen, striker and supports

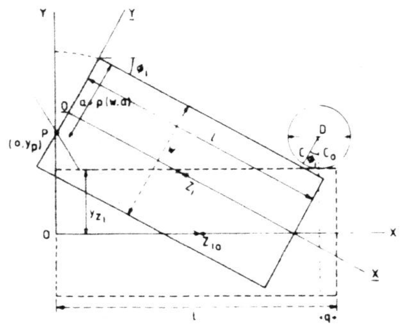

Fig. 2. Kinematic topography of impacted SENB-specimen. Situation is drawn, where impacted specimen - after having lost initial contact with striker and supports - hits the latter again.

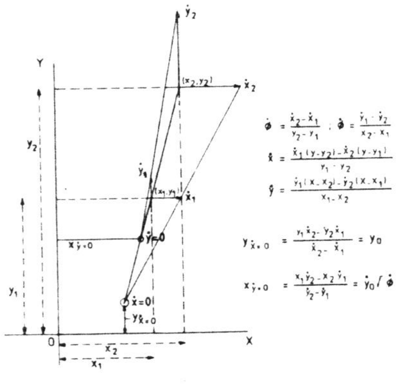

Fig. 3. Evaluation of $\dot{\phi}$ and $y_{\dot{x}=o}$ from $\dot{x}_1$ and $\dot{x}_2$ and of $\dot{\phi}$ and $x_{\dot{y}=o}$ from $\dot{y}_1$ and $\dot{y}_2$ resp.

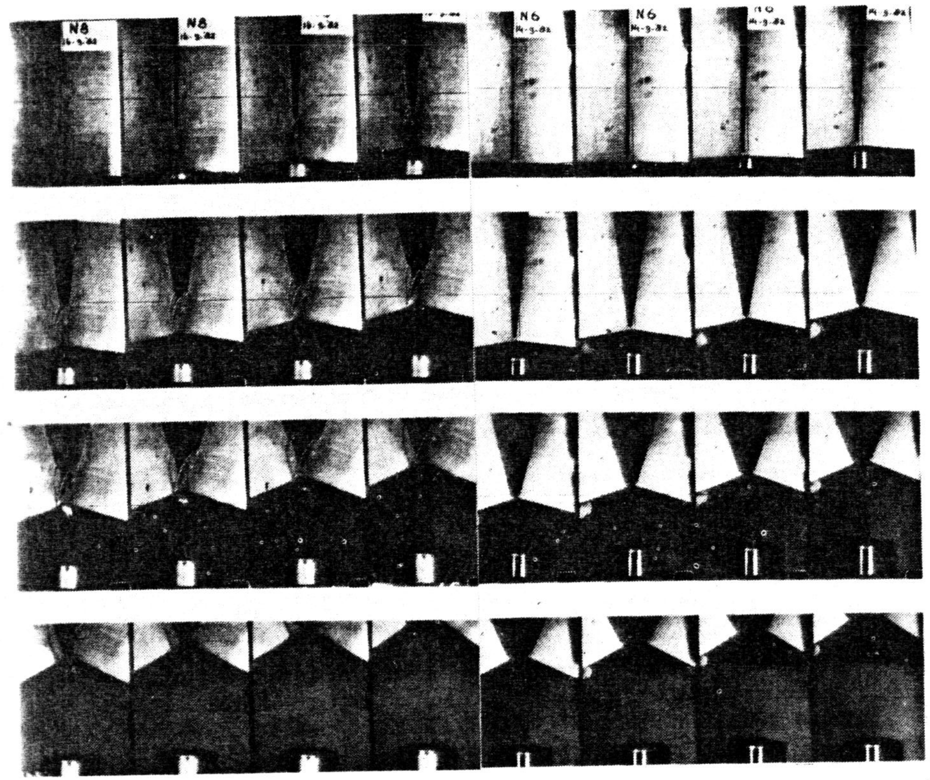

a. HY130-nr. 8; a_o=75 mm; 103.4 μs/f; 2^{nd} picture at t = 100 μs

b. HY130-nr. 6; a_o=99 mm; 102.0 μs/f; 2^{nd} picture at t = 60 μs

Fig. 4. 16 consecutive pictures of impacted HY130 steel specimens

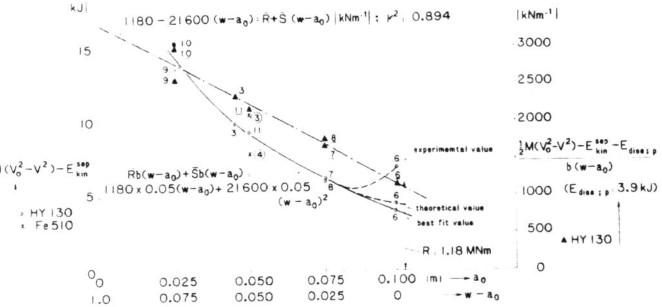

Fig. 5. Dissipated energy and average dissipated energy per unit crack area increase at separation of impacted SENB-specimens versus initial crack size

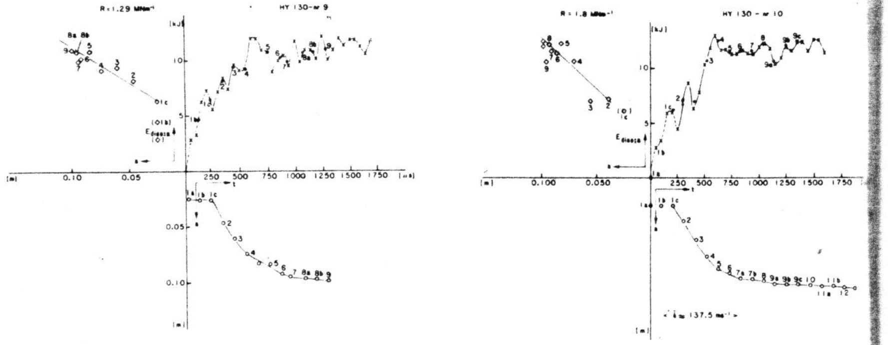

a. HY130-nr. 9; a_o = 25 mm b. HY130-nr. 10; a_o = 25 mm

Fig. 6. Dissipated energy and cracklength versus time and dissipated energy versus cracklength during tearing of impacted SENB-specimens

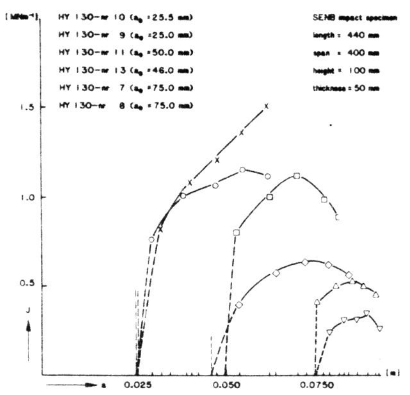

Fig. 7. J/Δa-curves for impacted HY130-steel SENB-specimens (with a_o as parameter)

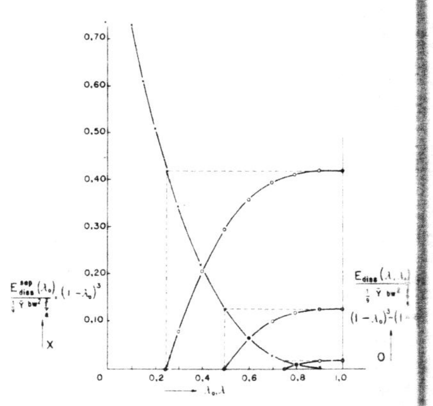

Fig. 8. Normalised dissipated energ at crack extension and separation for impacted HY130-steel SENB-specimens function of λ and λ_o resp. under limit moment conditi